European Journal of Radiology 115 (2019) 10–15

Contents lists available at ScienceDirect

European Journal of Radiology

journal homepage: www.elsevier.com/locate/ejrad

Research article

Radiomics for predicting hematoma expansion in patients with hypertensive intraparenchymal hematomas

Chao Ma[a,1], Yupeng Zhang[a,1], Tuerdialimu Niyazi[b,**], Jian Wei[c], Guo Guocai[c], Jianan Liu[b], Shikai Liang[d], Fei Liang[a], Peng Yan[a], Kun Wang[a,***], Chuhan Jiang[a,*]

[a] Department of Interventional Neuroradiology, Beijing Neurosurgical Institute and Beijing Tiantan Hospital, Capital Medical University, Beijing, China
[b] Department of Neurosurgery, Hetian Region People's Hospital, Xinjiang Uyghur Autonomous Region, China
[c] Department of Neurosurgery, Weifang TCM Hospital, Shandong, China
[d] Department of Neurosurgery, Beijing Tsinghua Changgeng Hospital, School of Clinical Medicine, Tsinghua University, Beijing, China

ARTICLE INFO

Keywords:
Radiomics
Computed tomography
Hematoma expansion
Hypertension
Machine learning

ABSTRACT

Purpose: To explore the feasibility of predicting hematoma expansion at acute phase via a radiomics approach.
Methods: 254 cases with hypertensive intraparenchymal hematomas were retrospectively reviewed. Baseline non-contrast enhanced CT scan (NECT) were obtained on admission and compared to follow up CT to confirm the occurrence of hematoma expansion. Cases were split into training dataset with 149 cases and a test dataset with 105 cases. Radiomics features were extracted and informative features were selected by least absolute shrinkage and selection operator (LASSO) with 3-fold-cross validation. A radiomics score was then constructed with the selected features to discriminate enlarged hematomas from those that remained stable. Discriminative performance of the score was evaluated on the training and test dataset with area under the curve (AUC) and confusion matrix related metrics.
Results: A total of 576 radiomics features were extracted from 6 feature groups on NECT, of which 484 were stable. 5 features were selected by LASSO and based on which a radiomics score were constructed. The radiomics score achieved high discrimination ability between hematoma expansion and no-expansion with AUC of 0.892 (95% CI: 0.824–0.959) and accuracy of 0.852 in the training dataset. In the test dataset, predicting sensitivity, specificity, PPV, NPV and accuracy were 0.808, 0.835, 0.618, 0.930 and 0.820, respectively.
Conclusions: Radiomics features were effective in the prediction of hematoma expansion for patients with hypertensive intraparenchymal hematomas. Our radiomics score may provide a fast and quantitative risk assessment for these patients.

1. Introduction

The worldwide incidence of hypertensive intracerebral hemorrhage (ICH) was 10–30 per 100 000 population [1], accounting for 10–15% of all strokes [2,3]. Most of the hematomas locate at the basal ganglia region, resulting in high rate of morbidity and the mortality within 30 days [4,5]. A frequently seen phenomenon in hypertensive ICH is hematoma expansion (HE), which occurs in about a third of ICH patients and greatly deteriorate their neurological outcomes [6–8]. Therefore, early identification of patients at high risks enables preventative interventions like blood pressure control, application of thrombin and surgical hemostatic, thus effectively improve outcomes [9,10].

Recently, there has been an avid research into the prediction of HE based on clinical and radiographic characteristics. Factors like hypertension [11], shorter time to computed tomography (CT) and use of warfarin [12] have been identified as independent clinical predictors of

Abbreviations: NECT, non-contrast enhanced CT; LASSO, least absolute shrinkage and selection operator; HE, hematoma expansion; NHE, no hematoma expansion; CTA, CT angiography; ICH, intracerebral hemorrhage; AUC, area under the curve; ICC, intraclass correlation coefficient; ROC, receiver operating characteristics curve; LoG, laplacian of gaussian; PPV, positive predictive value; NPV, negative predictive value; ROI, region of interest; GLCM, gray-level co-occurrence matrix; GLRLM, gray-level run length matrix

* Corresponding author at: Room 603, Beijing Neurosurgical Institute, No. 6 Tiantan Xili, Dongcheng District, Beijing, China.
** Corresponding author at: Department of Neurosurgery, No. 103 Wenhua Road, Hetian City, Xinjiang Uyghur Autonomous Region, China.
*** Corresponding author at: Room 617, Beijing Neurosurgical Institute, No. 6 Tiantan Xili, Dongcheng District, Beijing, China.
E-mail addresses: tuerdialimuniyazi@163.com (T. Niyazi), wangkun650@126.com (K. Wang), jiangchuhan126@126.com (C. Jiang).
[1] Chao Ma and Yupeng Zhang contributed equally.

https://doi.org/10.1016/j.ejrad.2019.04.001
Received 19 October 2018; Received in revised form 26 January 2019; Accepted 1 April 2019

HE. Besides, radiological signs on CT and CT angiography including spot sign [13,14], island sign [15], blend sign [16,17], black hole sign [18] and swirl sign [19] have also manifested adequate predictive power. Nevertheless, qualitative radiological signs are susceptible to intra and interobserver variability, lacking reproducibility among evaluators.

Radiomics is a newly developed tool that allows a high-throughput extraction of features from various modalities of images and enables us to conduct quantitative analysis of image features [20–22]. Since the aforementioned CT signs reflect that enlarged hematomas are prone to be more heterogenous in shape, texture and signal intensities, we hypothesize that enlarged hematomas can be screened out precisely if we can quantify the heterogeneity with the aid of radiomics features. Therefore, we conducted this study to explore the feasibility of predicting hematoma expansion at acute phase via a radiomics approach.

2. Methods

2.1. Patient's demographics and data acquisition

In total, we retrospectively reviewed 254 cases with hypertensive intraparenchymal hematomas. Hematomas located at cerebellum/brainstem and patients on anticoagulation/antiplatelet therapy were excluded. The occurrence rates of hematoma expansion were not significantly different between the training dataset and test dataset (21.5% vs 24.8%, P = 0.643). The training dataset comprised 102 males and 47 females (median age, 55.0; IQR, 47.0–64.0), and the test dataset included 56 males and 49 females (median age, 63.0; IQR, 55.0–71.0). Both in the training and test dataset, there were no significant statistical differences in age and gender between HE and NHE group. (Table 1). The study was approved by the institutional ethics committee in all four centers and informed consents were obtained for all patients. NECTs and clinical variables of these cases were collected from 4 centers and cases were split into a training dataset with 149 cases (Beijing Tiantan Hospital & Hetian Region People's Hospital) and a test dataset with 105 cases (Weifang TCM Hospital & Penglai TCM Hospital). The rate of hematoma expansion was comparable between the training and test dataset (21.5% vs 24.8%).

Baseline NECT images were acquired within 6 h after the onset of symptoms with either Siemens or GE medical systems. The follow up CT was obtained 48 h within the acquisition of the baseline CT. Hematoma expansion was defined as a relative increase of volume more than 33% or an absolute increase greater than 12.5 mL from the initial volume [7]. The scanning energy was 120 or 140 KVP in different centers and smart mAs were used. Slice thickness was 5 mm and the pixel spacing was 0.45 × 0.45 mm^2 or 0.49 × 0.49 mm^2. To reduce the discrepancy of imaging parameters implemented in different hospitals, we resampled all voxels into 1.0 × 1.0 × 1.0 mm^3 before feature extraction.

2.2. Feature extraction and stability evaluation

Regions of hematoma were manually segmented on NECT scans by 2 neuroradiologists (Chao Ma and Yupeng Zhang). Then, a total of 576 radiomics features (Supplementary Table 1) were extracted automatically for each patient with the Pyradiomics module written in Python [23]. Extracted features belonged to 6 groups, including 18 first-order statistics features, 16 shape features, 22 gray-level co-occurrence matrix (GLCM) texture features, 16 gray-level run length matrix (GLRLM) texture features, 448 wavelet features and 56 Laplacian of Gaussian (LoG) filtered image features. Each feature was named by concatenating the image type from which the feature was extracted, feature group and feature name by underline. For example, Wavelet_HHL_glrlm_ShortRunEmphasis was a feature extracted from the wavelet_HHL image, glrlm group and the feature name was ShortRunEmphasis. To avoid inter-observer variations during the manual segmentation, we calculated the intraclass correlation coefficient (ICC) for each feature and only those with high stability (ICC > 0.8) entered following analysis [24]. Unstable features were listed in Supplementary Table 1

2.3. Selection of informative feature with LASSO and radiomics score construction

We performed feature selection using the Least Absolute Shrinkage and Selection Operator (LASSO) algorithm, which was a perfect regression model in that it efficiently reduced the number of features. Features with non-zero coefficients were selected and the radiomics score was then calculated with the following formula:

$$\text{Radiomics score} = (\Sigma \beta_i * X_i) + \text{Intercept } (i = 0, 1, 2, 3\ldots\ldots)$$

Where X_i represented the i^{th} selected feature and β_i was its coefficient.

We then applied Youden Index to find out the optimal cutoff point of radiomics score which can best discriminate the hematoma expansion group and non-expansion group. The cutoff point was the radiomics score which maximized the Youden's *J* statistic, which was defined as:

$$J = \text{sensitivity} + \text{specificity} - 1$$

2.4. Prediction performance evaluation of the radiomics score

On the training dataset, prediction performance was evaluated with area under the curve (AUC) of the receiver operating characteristics curve (ROC). Confusion matrix related metrics like sensitivity, specificity, positive predictive value (PPV), negative predictive value (NPV) and accuracy were also calculated. On the test dataset, the same cutoff point of radiomics score was applied and confusion matrix related metrics were used to evaluate the score's performance.

2.5. Statistics

For continuous variables, difference was calculated with student *t*-test or Mann-Whitney U test as appropriate. Continuous data were represented as mean ± standard deviation or as median with interquartile range depending on whether or not the data were normally distributed. Chi-square test was used for estimating the differences in

Table 1
Population demographics and hematoma volume characteristics.

Characteristics	HE in trainig dataset	NHE in trainig dataset	p	HE in test dataset	NHE in test dataset	p
Patients, No. (%)	32(21.5%)	117(78.5%)	——	26(24.8%)	79(75.2%)	——
Age, y, median, (IQR)	53.0(44.0-59.0)	55.0(49.0-65.0)	0.278	62.0(55.5-65.0)	63.0(56.0-63.4)	0.456
Sex, M/F	24/8	78/39	0.494	16/10	40/39	0.459
Hematoma Volume (mL), mean, SD	20.9(19.1)	31.6(22.4)	0.004	13.8(10.7)	21.5(19.2)	0.043
Hematoma 3D diameter (mm), mean, SD	49(18)	59(16)	0.005	46(11)	55(19)	0.021
Hematoma 2D diameter (mL), mean, SD	42(17)	52(16)	0.004	39(13)	47(18)	0.022

Abbreviations: No. (%), the numbers before parentheses represent the actual numbers and the numbers.
Within parentheses represent corresponding percentages; SD, Standard Deviation; IQR, Interquartile Range.

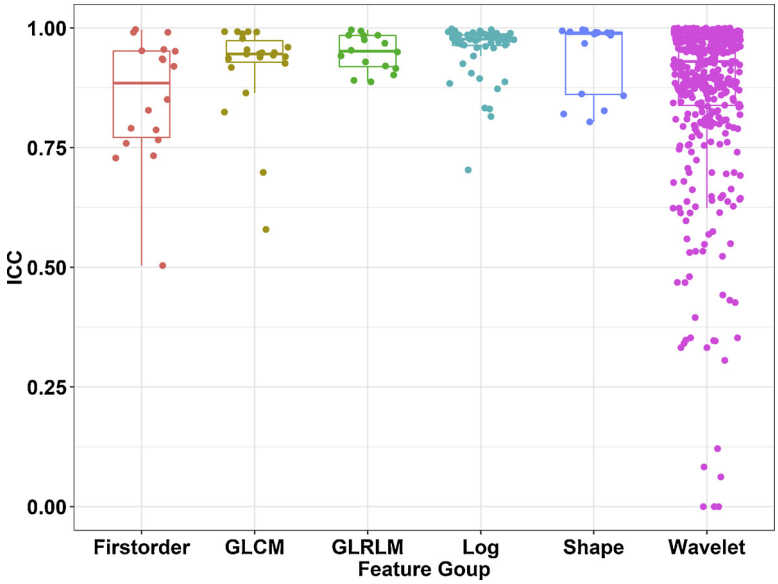

Fig. 1. Boxplot of ICC values for features extracted from 6 feature groups.

categorical variables and the results were listed in the form of number of events followed by relative frequencies (%). Statistical significance was defined as < 0.05. All statistics were performed with R software (version 3.4.3, R Foundation for Statistical Computing, Vienna, Austria). Additional R packages used in this study were 'glmnet', 'OptimalCutpoints' and 'ggplot2'.

3. Result

3.1. Hematoma characteristics

In the training dataset, hematoma volume (20.9 mL vs 31.6 mL, P = 0.004), 3D diameter (49 mm vs 59 mm, P = 0.005) and 2D diameter of hematoma (42 mL vs 52 mL, P = 0.004), were much smaller in the HE group. This was the same case in the test dataset, where hematomas were also much smaller in size (Table 1).

3.2. Selection of stable features

In Fig. 1, we illustrated the ICC value for each feature across all groups. All feature groups showed high stability, with the mean ICC value of features in each group exceeding 0.8. As shown in Table 2, the mean ICC of each group was as follows: shape features (ICC = 0.94 ± 0.08), first-order statistics (ICC = 0.85 ± 0.13), GLCM texture features (ICC = 0.92 ± 0.10), GLRLM texture features (ICC = 0.95 ± 0.04), LoG features (ICC = 0.96 ± 0.06) and wavelet features (ICC = 0.87 ± 0.17), respectively.

In total, 484 of the 576 (84%) extracted radiomics features showed high stability (ICC > 0.8), including 16 shape features (100%), 18 first-order statistics features (61%), 20 GLCM derived texture features (91%), 16 GLRLM derived texture features (100%), 55 LoG features (98%) and 366 Wavelet features (82%).

Table 2
Summary of selected feature numbers in each group and mean ICC.

Feature group	Feature number	Included number	Mean ICC
Shape	16	16 (100%)	0.94 ± 0.08
First-order	18	11(61%)	0.85 ± 0.13
GLCM	22	20(91%)	0.92 ± 0.10
GLRLM	16	16(100%)	0.95 ± 0.04
LoG	56	55(98%)	0.96 ± 0.06
Wavelet	448	366(82%)	0.87 ± 0.17

Abbreviations: GLCM, Gray-Level Co-occurrence Matrix; GLRLM, Gray-Level Run Length Matrix; LoG, Laplacian of Gaussian; ICC, Intraclass Correlation Coefficient.

3.3. Selection of informative features with LASSO and radiomics score construction

From the 484 stable radiomics features, 5 informative features with non-zero coefficients were finally selected by the LASSO algorithm (Fig. 2). On the training dataset, features were statistically different between the HE and NHE group except for the feature Autocorrelation in GLCM group (Wavelet_LLH image) (Table 3). With the 5 selected features, we constructed the radiomics score by multiplying the value of each feature with its coefficient and then sum all the 5 products with the intercept. In the training dataset, the radiomics scores ranged from -2.183 to 0.644, the mean radiomics score in the HE and non-HE group were -0.731 and -1.549, respectively. Optimal cutoff point of radiomics score for discriminating the 2 groups was calculated at -1.257. With this cutoff point, the radiomics score was able to predict hematoma expansion with accuracy at 0.852 and the AUC was 0.892 (95% CI: 0.824 − 0.959). On the training dataset, our score's sensitivity, specificity, positive predictive value (PPV) and negative predictive value (NPV) were 0.844, 0.855, 0.614 and 0.952, respectively (Fig. 3).

3.4. Performance validation of radiomics score on an independent test dataset

On the test dataset, the mean radiomics-score in HE and non-HE group were −0.698 and −1.454, which were significantly different in statistics ($P <$ 0.001). Besides, the radiomics score were stable on different dataset. For patients with hematoma expansion, radiomics scores between the training and test dataset showed no statistical difference (-0.731 vs -0.698, $P = 0.681$). This was the same case for patients without hematoma expansion, the radiomics scores were also similar between the training and test dataset (-1.549 vs -1.454, $P = 0.201$). Predictive performance of our radiomics score was then evaluated by confusion matrix on the test dataset. After applying the same cutoff point (-1.257), predicting sensitivity, specificity, PPV, NPV and accuracy reached 0.808, 0.835, 0.618, 0.930 and 0.820.

To further illustrate the radiomics score, we plot Fig. 4 in which the CT scan of two patients we showed. Case 1 had hematoma expansion on follow up CT scan who had a radiomics score at -1.093, which was

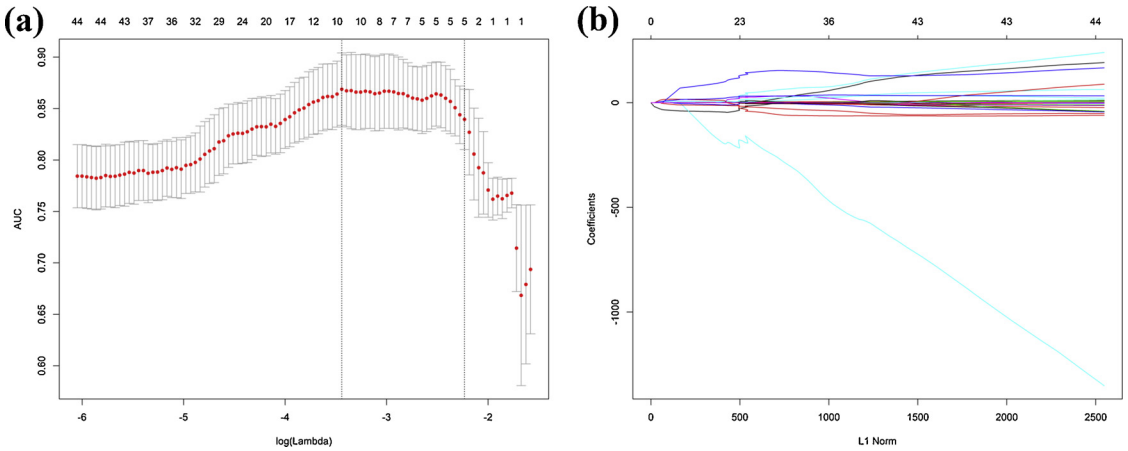

Fig. 2. Feature selection with LASSO. This method minimized the sum of squares of residues, with the sum of the absolute values of the selected features coefficients being not more than a tuning parameter (λ). Using 3-fold cross-validation to tune parameter (λ) selection in the LASSO model. (a) AUC was plotted versus log(λ). 5 Features with non-zero coefficients were selected using the minimum criteria. (b) LASSO coefficient profiles of the features. Each colored line represents the coefficient of each features.

bigger than the cutoff point. Case 2 had a relative stable hematoma, the radiomics score was lower than the cutoff point.

4. Discussion

In this retrospective study, we constructed a stable predictive model with 5 radiomics features extracted from NECT scan to predict HE. Favorable predictability was achieved in that the classification accuracy reached 0.852 in training dataset and 0.820 in the test dataset. Since NECT imaging is non-invasive, requiring no contrast injection and time-saving, this technique provided us with a fast and auxiliary approach to screen out patients at high risks of hematoma expansion.

Most recently, several radiographic signs were proposed for predicting HE on NECTs, including blend sign [16], island sign [15] and black hole sign [18]. Although these signs had very high predictive specificity, the sensitivity was relatively low, ranging from 31.9%–44.7%. The low sensitivity indicated that patients at risks of HE couldn't not be effectively selected out. Another useful radiographic marker was CTA spot sign, showing extravasation of contrast media or a bleeding artery in a hematoma [25,26], and was included in most of the currently available predicting scores [27–29]. The PREDICT cohort study evaluated its prediction ability, but the sensitivity was only 51% [13]. In the study of Orito, prediction sensitivity of spot sign reached 77.8%, higher than the previous report. However, the HE criteria was defined as 10% relative increment in volume, different from the widely recognized 33% increase criteria, lowering its comparability with other studies [14]. In a recent meta-analysis which explored the diagnostic value of spot sign, the pooled sensitivity was 62% [30]. Even though spot sign and spot sign number were combined with clinical predictors to construct predicting scores, like the 9-point score, PREDICT A and PREDICT B score. The AUC of these score were reported as 0.761, 0.823 and 0.804, which were only medium accurate [27].

Compared with these existing radiographic markers, our radiomics score showed improved predicting performances. On the training dataset, the sensitivity of the radiomics score was 0.844 and the AUC reached 0.892. On the test dataset, the sensitivity was 0.808. Another advantage of the radiomics score was its reproducibility. Even though good inter- and intra-observer agreement was achieved for these existing radiographic signs like the island sign, these signs were rated by experts in ICH imaging. It was still unclear if less experienced radiologists and clinical physicians could make a fast and accurate identification of these signs. In the radiomics score, the 5 selected quantitative features had ICC values over 0.8, which guaranteed the stability in calculating the feature value from the manually drawn region of interest (ROI). In the future, the manually drawn ROIs can be replaced by automatic segmentation of the hematomas, which will further eliminate subjective factors in making the predictions and thus elevate the consistency of results.

Existing radiographic markers, regardless of their difference in nomenclatures and manifestations, actually reflected the irregularity of the hematomas' shape and heterogeneity of hematomas' composition. Variations in hematomas' shape and density might reflect multifocal and active bleeding, which were regarded as the major underlying mechanism of HE. Previous studies also proved that shape and density heterogeneity were independent predictors of hematoma growth [31,32]. Recently, quantitative approaches have been attempted to evaluate the prediction power of computed hematoma density features. In the study of Barras et al., coefficient of variation of the hematoma attenuation was identified as a significant predictor of hematoma growth [33]. Another study evaluated how well the texture features extracted from images filtered by Laplacian of Gaussian bandpass can predict hematoma expansion and proved that the variance and uniformity of hematoma intensities were statistically different between HE and NHE patients [34]. In our study, we tested the predictive value of more radiomics features, including those extracted from the original image and those from wavelet filtered image, and combined with

Table 3
Values of the 5 selected radiomics features and score.

Characteristics	HE in training dataset	NHE in training dataset	p	HE in test dataset	NHE in test dataset	p
original_glrlm_GrayLevelNonUniformityNormalized	0.434(0.065)	0.389(0.045)	< 0.001	0.463(0.047)	0.415(0.048)	< 0.001
Wavelet_LLH_glcm_Autocorrelation	3.319 (3.189)	2.123(0.948)	0.559	2.307(2.068)	2.020(0.650)	0.804
Wavelet_LHL_glcm_Idmn	0.938(0.031)	0.969(0.018)	< 0.001	0.935(0.028)	0.966(0.023)	< 0.001
Wavelet_HHL_glrlm_ShortRunEmphasis	0.616(0.010)	0.603(0.026)	0.007	0.617(0.029)	0.612(0.015)	0.596
Wavelet_LLL_glrlm_GrayLevelNonUniformityNormalized	0.208(0.041)	0.186(0.017)	< 0.001	0.213(0.045)	0.182(0.020)	< 0.001
Radiomics-score, mean	−0.731	−1.549	< 0.001	−0.698	−1.454	< 0.001

Abbreviations: HE, Hematoma Expansion; NHE, No Hematoma Expansion.

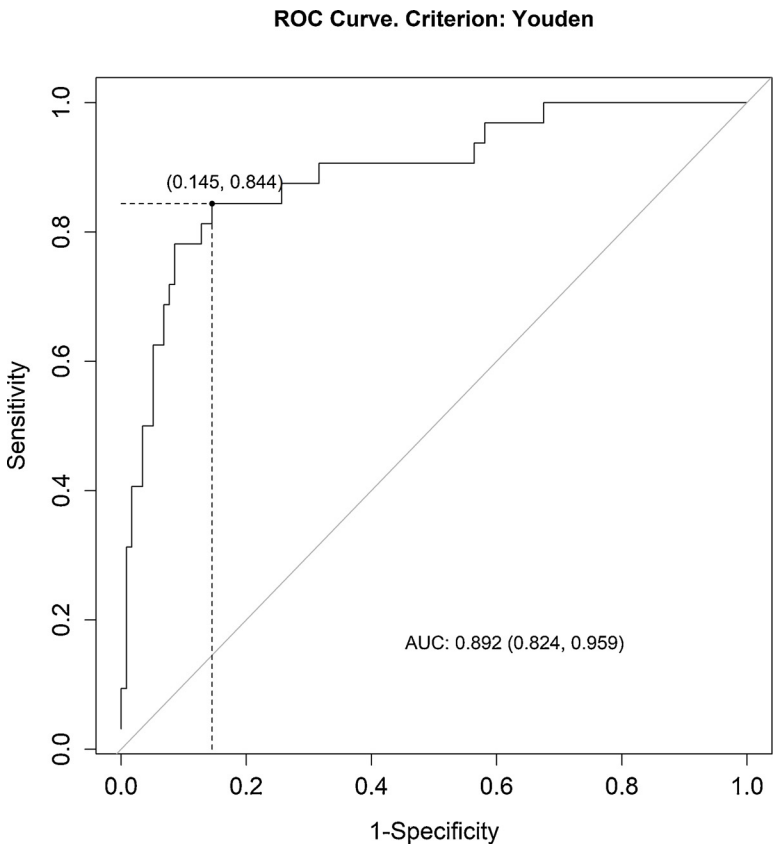

Fig. 3. Receiver operating characteristic (ROC) curves of the radiomics signature in training dataset. − 1.257 was the cutoff value of Radscore, and the corresponding specificity and sensitivity is shown in the bracket. Area under the receiver operating characteristic curve (AUC) and its 95% confidence interval were also demonstrated.

machine learning to select relevant features. In accordance with previous studies, included features like Idmn and GrayLevelNonUniformityNormalized all indicated that hematomas were more heterogeneous and had a lower similarity in intensity values.

In the training and test datasets, demographic and radiological characteristics of hematomas were matched between the HE and NHE group, except that hematoma size was smaller in the HE group than in the NHE group. The baseline hematoma volume was not incorporated into our final radiomics score, but several studies have recorded it as a potential predictor of HE, though with a contradicting effect. Most of the studies reported that larger volume of hematoma was associated with hematoma expansion. The 9-point prediction score for hematoma expansion included 4 individual components, namely, the use of warfarin sodium, time to initial CT, baseline ICH volume and CTA spot sign [12]. Hematoma volume entered the score as a tertiary variable (< 30, 30–60, or > 60 mL) and 3 points were allocated. The larger the volume, the higher the risk of hematoma expansion. On the contrary, in the cohort from which a 5-point BAT score was created, baseline hematoma volume was statistically smaller in HE group compared with the NHE group [35]. What's more, we thought that it was hard to fully elucidate the true influence of baseline hematoma volume on expansion, due to the fact that different study cohorts might include varied percentage of patients in the NHE group whose hematomas had already expanded before baseline CT scanning. A population-based cohort of patients with stratified time to baseline CT was needed to explore the true effect of hematoma volume on HE.

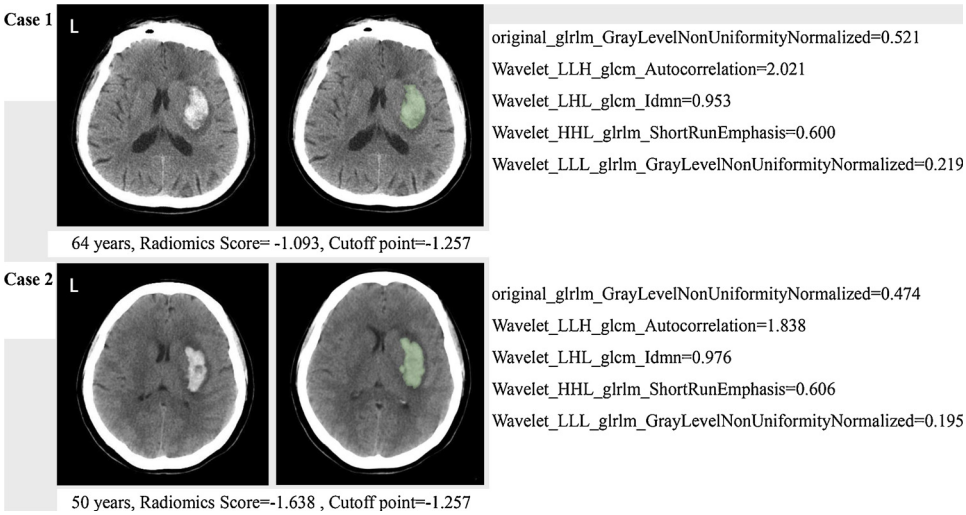

Fig. 4. NECT scan with hematoma masks for 2 cases with (case 1) and without (case 2) hematoma expansion. Case 1 had a radiomics score -1.093 and case 2 had a radiomics score -1.638. (Cutoff point of the radiomics score was -1.257, cases with radiomics score > -1.257 would be classified into HE group, while those with scores smaller than -1.257 would be classified into NHE group).

4.1. Limitation

The major limitations of the study rooted from the relative small size of the dataset, which on one side might influence the performance of the derived model on the training dataset and on the other side lowered the reliability of validation on the test dataset. Another limitation was due to the retrospective nature of the study, which resulted in the fact that different scanners were used. In the future, our model should be further tested on a population-based cohort of patients with CTs obtained using identical acquisition parameters.

5. Conclusion

We developed and externally validated a radiomics score for the prediction of hematoma expansion. The score was capable of predicting hematoma expansion on non-enhanced CT scans with adequate accuracy. Future studies should focus on further elevating the score's performance and comparing its efficacy with routine biomarkers like the spot sign on CT angiography.

Source of funding

This work was supported by the National Natural Science Foundation of China (Grant No. 81371314) and the High-level Personnel Training Program of Beijing Health system (Grant No. 2013-2-016).

Acknowledgement

None.

Appendix A. Supplementary data

Supplementary material related to this article can be found, in the online version, at doi:https://doi.org/10.1016/j.ejrad.2019.04.001.

References

[1] A.I. Qureshi, S. Tuhrim, J.P. Broderick, H.H. Batjer, H. Hondo, D.F. Hanley, Spontaneous intracerebral hemorrhage, N. Engl. J. Med. 344 (2001) 1450–1460.
[2] C.L. Sudlow, C.P. Warlow, Comparable studies of the incidence of stroke and its pathological types: results from an international collaboration. International stroke incidence collaboration, Stroke 28 (1997) 491–499.
[3] V.L. Feigin, C.M. Lawes, D.A. Bennett, C.S. Anderson, Stroke epidemiology: a review of population-based studies of incidence, prevalence, and case-fatality in the late 20th century, Lancet Neurol. 2 (2003) 43–53.
[4] B.M. Hansen, O.G. Nilsson, H. Anderson, B. Norrving, H. Saveland, A. Lindgren, Long term (13 years) prognosis after primary intracerebral haemorrhage: a prospective population based study of long term mortality, prognostic factors and causes of death, J. Neurol. Neurosurg. Psychiatry 84 (2013) 1150–1155.
[5] M.T. Poon, A.F. Fonville, R. Al-Shahi Salman, Long-term prognosis after intracerebral haemorrhage: systematic review and meta-analysis, J. Neurol. Neurosurg. Psychiatry 85 (2014) 660–667.
[6] S.M. Davis, J. Broderick, M. Hennerici, N.C. Brun, M.N. Diringer, S.A. Mayer, et al., Hematoma growth is a determinant of mortality and poor outcome after intracerebral hemorrhage, Neurology 66 (2006) 1175–1181.
[7] C. Delcourt, Y. Huang, H. Arima, J. Chalmers, S.M. Davis, E.L. Heeley, et al., Hematoma growth and outcomes in intracerebral hemorrhage: the interact1 study, Neurology 79 (2012) 314–319.
[8] Y. Fujii, R. Tanaka, S. Takeuchi, T. Koike, T. Minakawa, O. Sasaki, Hematoma enlargement in spontaneous intracerebral hemorrhage, J. Neurosurg. 80 (1994) 51–57.
[9] C.S. Anderson, E. Heeley, Y. Huang, J. Wang, C. Stapf, C. Delcourt, et al., Rapid blood-pressure lowering in patients with acute intracerebral hemorrhage, N. Engl. J. Med. 368 (2013) 2355–2365.
[10] A.I. Qureshi, Y.Y. Palesch, W.G. Barsan, D.F. Hanley, C.Y. Hsu, R.L. Martin, et al., Intensive blood-pressure lowering in patients with acute cerebral hemorrhage, N. Engl. J. Med. 375 (2016) 1033–1043.
[11] J.S. Balami, A.M. Buchan, Complications of intracerebral haemorrhage, Lancet Neurol. 11 (2012) 101–118.
[12] H.B. Brouwers, Y. Chang, G.J. Falcone, X. Cai, A.M. Ayres, T.W. Battey, et al., Predicting hematoma expansion after primary intracerebral hemorrhage, JAMA Neurol. 71 (2014) 158–164.
[13] A.M. Demchuk, D. Dowlatshahi, D. Rodriguez-Luna, C.A. Molina, Y.S. Blas, I. Dzialowski, et al., Prediction of haematoma growth and outcome in patients with intracerebral haemorrhage using the ct-angiography spot sign (predict): a prospective observational study, Lancet Neurol. 11 (2012) 307–314.
[14] K. Orito, M. Hirohata, Y. Nakamura, N. Takeshige, T. Aoki, G. Hattori, et al., Leakage sign for primary intracerebral hemorrhage: a novel predictor of hematoma growth, Stroke 47 (2016) 958–963.
[15] Q. Li, Q.J. Liu, W.S. Yang, X.C. Wang, L.B. Zhao, X. Xiong, et al., Island sign: an imaging predictor for early hematoma expansion and poor outcome in patients with intracerebral hemorrhage, Stroke 48 (2017) 3019–3025.
[16] Q. Li, G. Zhang, Y.J. Huang, M.X. Dong, F.J. Lv, X. Wei, et al., Blend sign on computed tomography: novel and reliable predictor for early hematoma growth in patients with intracerebral hemorrhage, Stroke 46 (2015) 2119–2123.
[17] P.B. Sporns, M. Schwake, R. Schmidt, A. Kemmling, J. Minnerup, W. Schwindt, et al., Computed tomographic blend sign is associated with computed tomographic angiography spot sign and predicts secondary neurological deterioration after intracerebral hemorrhage, Stroke 48 (2017) 131–135.
[18] Q. Li, G. Zhang, X. Xiong, X.C. Wang, W.S. Yang, K.W. Li, et al., Black hole sign: novel imaging marker that predicts hematoma growth in patients with intracerebral hemorrhage, Stroke 47 (2016) 1777–1781.
[19] D. Ng, L. Churilov, P. Mitchell, R. Dowling, B. Yan, The ct swirl sign is associated with hematoma expansion in intracerebral hemorrhage, AJNR Am. J. Neuroradiol. 39 (2018) 232–237.
[20] R.J. Gillies, P.E. Kinahan, H. Hricak, Radiomics: images are more than pictures, they are data, Radiology 278 (2016) 563–577.
[21] V. Kumar, Y. Gu, S. Basu, A. Berglund, S.A. Eschrich, M.B. Schabath, et al., Radiomics: the process and the challenges, Magn. Reson. Imaging 30 (2012) 1234–1248.
[22] P. Lambin, E. Rios-Velazquez, R. Leijenaar, S. Carvalho, R.G. van Stiphout, P. Granton, et al., Radiomics: extracting more information from medical images using advanced feature analysis, Eur. J. Cancer 48 (2012) 441–446.
[23] J.J.M. van Griethuysen, A. Fedorov, C. Parmar, A. Hosny, N. Aucoin, V. Narayan, et al., Computational radiomics system to decode the radiographic phenotype, Cancer Res. 77 (2017) e104–e107.
[24] H.J. Aerts, E.R. Velazquez, R.T. Leijenaar, C. Parmar, P. Grossmann, S. Carvalho, et al., Decoding tumour phenotype by noninvasive imaging using a quantitative radiomics approach, Nat. Commun. 5 (4006) (2014).
[25] J.E. Delgado Almandoz, H.R. Kelly, P.W. Schaefer, H.B. Brouwers, A.J. Yoo, M.J. Stone, et al., Ct angiography spot sign predicts in-hospital mortality in patients with secondary intracerebral hemorrhage, J. Neurointerv. Surg. 4 (2012) 442–447.
[26] H.B. Brouwers, J.N. Goldstein, J.M. Romero, J. Rosand, Clinical applications of the computed tomography angiography spot sign in acute intracerebral hemorrhage: a review, Stroke 43 (2012) 3427–3432.
[27] T.J. Huynh, R.I. Aviv, D. Dowlatshahi, D.J. Gladstone, A. Laupacis, A. Kiss, et al., Validation of the 9-point and 24-point hematoma expansion prediction scores and derivation of the predict a/b scores, Stroke 46 (2015) 3105–3110.
[28] J.E. Delgado Almandoz, A.J. Yoo, M.J. Stone, P.W. Schaefer, J.N. Goldstein, J. Rosand, et al., Systematic characterization of the computed tomography angiography spot sign in primary intracerebral hemorrhage identifies patients at highest risk for hematoma expansion: the spot sign score, Stroke 40 (2009) 2994–3000.
[29] X. Wang, H. Arima, R. Al-Shahi Salman, M. Woodward, E. Heeley, C. Stapf, et al., Clinical prediction algorithm (brain) to determine risk of hematoma growth in acute intracerebral hemorrhage, Stroke 46 (2015) 376–381.
[30] X. Xu, J. Zhang, K. Yang, Q. Wang, B. Xu, X. Chen, Accuracy of spot sign in predicting hematoma expansion and clinical outcome: a meta-analysis, Medicine (Baltimore) 97 (2018) e11945.
[31] C.D. Barras, B.M. Tress, S. Christensen, L. MacGregor, M. Collins, P.M. Desmond, et al., Density and shape as ct predictors of intracerebral hemorrhage growth, Stroke 40 (2009) 1325–1331.
[32] D. Zhang, J. Chen, J. Guo, Y. Jiang, Y. Dong, B. Ping-Chi Chen, et al., Hematoma heterogeneity on noncontrast computed tomography predicts intracerebral hematoma expansion: a meta-analysis, World Neurosurg. 114 (2018) e663–e676.
[33] C.D. Barras, B.M. Tress, S. Christensen, M. Collins, P.M. Desmond, B.E. Skolnick, et al., Quantitative ct densitometry for predicting intracerebral hemorrhage growth, AJNR Am. J. Neuroradiol. 34 (2013) 1139–1144.
[34] Q. Shen, Y. Shan, Z. Hu, W. Chen, B. Yang, J. Han, et al., Quantitative parameters of ct texture analysis as potential markersfor early prediction of spontaneous intracranial hemorrhage enlargement, Eur. Radiol. 28 (2018) 4389–4396.
[35] A. Morotti, D. Dowlatshahi, G. Boulouis, F. Al-Ajlan, A.M. Demchuk, R.I. Aviv, et al., Predicting intracerebral hemorrhage expansion with noncontrast computed tomography: the bat score, Stroke 49 (2018) 1163–1169.